

# Effect of tensor couplings in a relativistic Hartree approach for finite nuclei

Guangjun Mao

<sup>1)</sup>*Institute of High Energy Physics, Chinese Academy of Science*

*P.O. Box 918(4), Beijing 100039, P.R. China*<sup>1</sup>

<sup>2)</sup>*Institute of Theoretical Physics, Chinese Academy of Science*

*P.O. Box 2735, Beijing 100080, P.R. China*

<sup>3)</sup>*CCAST (World Lab.), P.O. Box 8730, Beijing 100080, P.R. China*

## Abstract

The relativistic Hartree approach describing the bound states of both nucleons and anti-nucleons in finite nuclei has been extended to include tensor couplings for the  $\omega$ - and  $\rho$ -meson. After readjusting the parameters of the model to the properties of spherical nuclei, the effect of tensor-coupling terms rises the spin-orbit force by a factor of 2, while a large effective nucleon mass  $m^*/M_N \approx 0.8$  sustains. The overall nucleon spectra of shell-model states are improved evidently. The predicted anti-nucleon spectra in the vacuum are deepened about 20 – 30 MeV.

**PACS** number(s): 21.10.-k; 21.60.-n; 13.75.Cs

---

<sup>1</sup>mailing address

e-mail: maogj@mail.ihep.ac.cn

## I. INTRODUCTION

One of the main characters distinguishing relativistic approaches from nonrelativistic approaches is that the former one has a vacuum. It is quite interesting to study the structure of quantum vacuum in a many-body system, e.g., in a finite nucleus where the Fermi sea is filled with the valence nucleons while the Dirac sea is full of the nucleon–anti-nucleon pairs. In the relativistic treatment of nuclear phenomena [1], the Dirac equation is used to describe the behavior of nucleons in nuclei. The effects of the nuclear medium on nucleons are taken into account through introducing strong Lorentz scalar ( $S$ ) and time-component Lorentz vector ( $V$ ) potential. In the language of meson-exchange theory the scalar potential can be attributed to the exchange of sigma meson and the vector potential to the exchange of omega and rho mesons as well as the electromagnetic force. Since the Dirac equation describes the nucleon and the anti-nucleon simultaneously, the effects of mean fields act on both of them. Consequently, not only the valence nucleons are bounded in the shell-model like states, but also there exist bound states for anti-nucleons emerging from the lower continuum. The observation of anti-nucleon bound states is a verification for the application of the Dirac phenomenology to a relativistic many-body system [2]. It constitutes a basis for the widely used relativistic mean-field (RMF) theory [1, 3, 4, 5, 6, 7] and the relativistic Hartree approach (RHA) [8, 9, 10, 11, 12]. Since the bound states of nucleons are subject to the cancellation of two potentials  $S + V$  ( $V$  is positive,  $S$  is negative) while the bound states of anti-nucleons, due to the G-parity, are sensitive to the sum of them  $S - V$ , consistent studies of both the nucleon and the anti-nucleon bound states can determine the individual  $S$  and  $V$ . In addition, the exact knowledge of potential depth for anti-nucleons in the medium is a prerequisite for the study of anti-matter and anti-nuclei in relativistic heavy-ion collisions [13, 14].

The shell-model states have been theoretically and experimentally well established [15] while no information for the bound states of anti-nucleons in the Dirac sea are available. This is the aim of our work. In Ref. [16] we have developed a relativistic Hartree approach which describes the bound states of nucleons and anti-nucleons consistently. The

contributions of the Dirac sea to the source terms of meson-field equations are considered up to the one-nucleon loop and one-meson loop and evaluated by means of the derivative expansion technique [17]. The parameters of the model are adjusted by fitting to the properties of spherical nuclei. The major outcome of the RHA model is that a rather large effective nucleon mass  $m^*/M_N \approx 0.8$  is obtained compared to the value of 0.6 in the relativistic mean-field calculations where the *no-sea* approximation is adopted. This is caused by the effects of the vacuum contributions which decrease the magnitude of the scalar potential  $S$  substantially. Correspondingly, the vector potential  $V$  is also suppressed since the quantity  $V + S$  is controlled by the saturation properties. As pointed out above, the anti-nucleon bound states are mainly determined by the sum of the scalar and vector potentials  $S - V$ . The smaller values of  $S$  and  $V$  obtained in the RHA calculations lead to a weaker bound on the single-particle energies of anti-nucleons, which turn out to be only half of that computed in the RMF model. On the other hand, the spin-orbit potential of nucleons is related to  $d(S - V)/dr$ . In the RHA calculations the spin-orbit splitting of the shell-model states is roughly 1/3 of that calculated in the RMF approach and indicated by the empirical data, although the general trend of the energy spectra coincides with each other. Because our goal is to develop a model to predict the bound states of anti-nucleons in the vacuum with the model parameters constrained by the nuclear bulk properties, in order to get reliable results for the anti-nucleon spectra one should first describe the nucleon spectra as good as possible.

Theoretically one can incorporate tensor couplings for the  $\omega$ - and  $\rho$ -meson, which mainly contribute to the spin-orbit force. The model now becomes non-renormalizable. However, from the point of view of modern effective field theory [18] the argument of renormalizability is not a severe restriction to theories. Since we will employ an effective Lagrangian of mesonic degrees of freedom and nucleons, just as the Skyrme force is an effective Lagrangian for nonrelativistic calculations [19], the mesons here are effective mesons. In an effective field theory one normally evaluates the lowest-order diagrams and makes regularization whenever a divergence appears. The parameters of the Lagrangian are adjusted to fit certain experimental data. The validity of the whole approach is

justified by successful explanations and predictions of observables. In other words, within the framework of an effective field theory one mainly concerns the balance between the predictive ability of the theory and the complexity of the theory.

In the present work we will investigate the effects of tensor couplings in the relativistic Hartree approach for finite nuclei. In this extended version of the model the parameters will be rearranged in a least-square fit to the properties of spherical nuclei. The model is then applied to study the bound states of nucleons and anti-nucleons. The paper is organized as follows: In Sect. II we introduce the effective Lagrangian and review the RHA model. In Sect. III we present the numerical results and discussions. A summary and outlook are finally given in Sect. IV.

## II. RELATIVISTIC HARTREE APPROACH

The Lagrangian density of nucleons interacting through the exchange of mesons can be expressed as [1]

$$\mathcal{L} = \mathcal{L}_F + \mathcal{L}_I. \quad (1)$$

Here  $\mathcal{L}_F$  is the Lagrangian density for free nucleon, mesons and photon

$$\begin{aligned} \mathcal{L}_F = & \bar{\psi} [i\gamma_\mu \partial^\mu - M_N] \psi + \frac{1}{2} \partial_\mu \sigma \partial^\mu \sigma - U(\sigma) - \frac{1}{4} \omega_{\mu\nu} \omega^{\mu\nu} \\ & + \frac{1}{2} m_\omega^2 \omega_\mu \omega^\mu - \frac{1}{4} \mathbf{R}_{\mu\nu} \cdot \mathbf{R}^{\mu\nu} + \frac{1}{2} m_\rho^2 \mathbf{R}_\mu \cdot \mathbf{R}^\mu - \frac{1}{4} A_{\mu\nu} A^{\mu\nu} \end{aligned} \quad (2)$$

and  $U(\sigma)$  is the self-interaction part of the scalar field [20]

$$U(\sigma) = \frac{1}{2} m_\sigma^2 \sigma^2 + \frac{1}{3!} b \sigma^3 + \frac{1}{4!} c \sigma^4. \quad (3)$$

In the above expressions  $\psi$  is the Dirac spinor of the nucleon;  $\sigma$ ,  $\omega_\mu$ ,  $\mathbf{R}_\mu$  and  $A_\mu$  represent the scalar meson, vector meson, isovector-vector meson field and the electromagnetic field, respectively. Here the field tensors for the omega, rho and photon are given in terms of their potentials by

$$\omega_{\mu\nu} = \partial_\mu \omega_\nu - \partial_\nu \omega_\mu, \quad (4)$$

$$\mathbf{R}_{\mu\nu} = \partial_\mu \mathbf{R}_\nu - \partial_\nu \mathbf{R}_\mu, \quad (5)$$

$$A_{\mu\nu} = \partial_\mu A_\nu - \partial_\nu A_\mu. \quad (6)$$

$\mathcal{L}_I$  is the interaction Lagrangian density

$$\begin{aligned}\mathcal{L}_I = & g_\sigma \bar{\psi} \psi \sigma - g_\omega \bar{\psi} \gamma_\mu \psi \omega^\mu - \frac{f_\omega}{4M_N} \bar{\psi} \sigma^{\mu\nu} \psi \omega_{\mu\nu} - \frac{1}{2} g_\rho \bar{\psi} \gamma_\mu \boldsymbol{\tau} \cdot \psi \mathbf{R}^\mu \\ & - \frac{f_\rho}{8M_N} \bar{\psi} \sigma^{\mu\nu} \boldsymbol{\tau} \cdot \psi \mathbf{R}_{\mu\nu} - \frac{1}{2} e \bar{\psi} (1 + \tau_0) \gamma_\mu \psi A^\mu.\end{aligned}\quad (7)$$

Here  $\sigma_{\mu\nu} = \frac{i}{2} [\gamma_\mu, \gamma_\nu]$ ,  $\boldsymbol{\tau}$  is the isospin operator of the nucleon and  $\tau_0$  is its third component.  $g_\sigma$ ,  $g_\omega$ ,  $g_\rho$  and  $e^2/4\pi = 1/137$  are the coupling strengths for the  $\sigma$ -,  $\omega$ -,  $\rho$ -meson and for the photon, respectively.  $f_\omega$  and  $f_\rho$  are the tensor-coupling strengths of vector mesons.  $M_N$  is the free nucleon mass and  $m_\sigma$ ,  $m_\omega$ ,  $m_\rho$  are the masses of the  $\sigma$ -,  $\omega$ -, and  $\rho$ -meson.

In finite nuclei the Dirac equation is written as

$$\begin{aligned}i \frac{\partial}{\partial t} \psi(\mathbf{x}, t) = & \left[ -i \boldsymbol{\alpha} \cdot \boldsymbol{\nabla} + \beta (M_N - g_\sigma \sigma(\mathbf{x})) + g_\omega \omega_0(\mathbf{x}) - \frac{f_\omega}{2M_N} i \boldsymbol{\gamma} \cdot (\boldsymbol{\nabla} \omega_0(\mathbf{x})) \right. \\ & \left. + \frac{1}{2} g_\rho \tau_0 R_{0,0}(\mathbf{x}) - \frac{f_\rho}{4M_N} i \tau_0 \boldsymbol{\gamma} \cdot (\boldsymbol{\nabla} R_{0,0}(\mathbf{x})) + \frac{1}{2} e (1 + \tau_0) A_0(\mathbf{x}) \right] \psi(\mathbf{x}, t).\end{aligned}\quad (8)$$

The field operator can be expanded according to nucleons and anti-nucleons and reads as

$$\psi(\mathbf{x}, t) = \sum_{\alpha} \left[ b_{\alpha} \psi_{\alpha}(\mathbf{x}) e^{-iE_{\alpha}t} + d_{\alpha}^+ \psi_{\alpha}^a(\mathbf{x}) e^{i\bar{E}_{\alpha}t} \right].\quad (9)$$

Here the label  $\alpha$  denotes the full set of single-particle quantum numbers.  $\psi_{\alpha}(\mathbf{x})$  are the wave functions of nucleons and  $\psi_{\alpha}^a(\mathbf{x})$  are those of anti-nucleons;  $E_{\alpha}$  and  $\bar{E}_{\alpha}$  are their positive energies, respectively.  $b_{\alpha}$  and  $d_{\alpha}^+$  are the annihilation and creation operators of nucleons and anti-nucleons that satisfy the standard anticommutation relations. We assume that the meson fields depend only on the radius and discuss the problem in spherically symmetric nuclei. In this case, the usual angular momentum and parity are good quantum numbers. As described in Refs. [21, 22], the eigenfunctions of nucleons are the well-known spherical spinors

$$\psi_{\alpha}(\mathbf{x}) = \begin{pmatrix} i \frac{G_{\alpha}(r)}{r} \Omega_{jlm}(\frac{\mathbf{r}}{r}) \\ \frac{F_{\alpha}(r)}{r} \frac{\boldsymbol{\sigma} \cdot \mathbf{r}}{r} \Omega_{jlm}(\frac{\mathbf{r}}{r}) \end{pmatrix}.\quad (10)$$

We make the ansatz for the wave functions of anti-nucleons [16]

$$\psi_{\alpha}^a(\mathbf{x}) = \begin{pmatrix} \frac{\bar{F}_{\alpha}(r)}{r} \frac{\boldsymbol{\sigma} \cdot \mathbf{r}}{r} \Omega_{jlm}(\frac{\mathbf{r}}{r}) \\ i \frac{\bar{G}_{\alpha}(r)}{r} \Omega_{jlm}(\frac{\mathbf{r}}{r}) \end{pmatrix}.\quad (11)$$

Here  $\Omega_{jlm}$  are the spherical spinors defined as

$$\Omega_{jlm} = \sum_{m'm_s} \left( l \frac{1}{2} j \mid m'm_s m \right) Y_{lm'} \chi_{\frac{1}{2} m_s}, \quad (12)$$

$Y_{lm'}$  are the spherical harmonics and  $\chi_{\frac{1}{2} m_s}$  are the eigenfunctions of the spin operators.  $G_\alpha$ ,  $F_\alpha$  and  $\bar{F}_\alpha$ ,  $\bar{G}_\alpha$  are the remaining *real* radial wave functions of nucleons and anti-nucleons for upper and lower components, respectively.

Inserting Eq. (9) into Eq. (8) one immediately obtains two relativistic wave equations for the  $\psi_\alpha(\mathbf{x})$  and  $\psi_\alpha^a(\mathbf{x})$ . Applying the concrete expressions of the wave functions given in (10) and (11), we arrive at the coupled equations for the radial wave functions of nucleons

$$\begin{aligned} E_\alpha G_\alpha(r) &= \left[ -\frac{d}{dr} + \frac{\kappa_\alpha}{r} - \frac{f_\omega}{2M_N} (\partial_r \omega_0(r)) - \frac{f_\rho}{4M_N} \tau_{0\alpha} (\partial_r R_{0,0}(r)) \right] F_\alpha(r) \\ &\quad + \left[ M_N - g_\sigma \sigma(r) + g_\omega \omega_0(r) + \frac{1}{2} g_\rho \tau_{0\alpha} R_{0,0}(r) \right. \\ &\quad \left. + \frac{1}{2} e (1 + \tau_{0\alpha}) A_0(r) \right] G_\alpha(r), \end{aligned} \quad (13)$$

$$\begin{aligned} E_\alpha F_\alpha(r) &= \left[ \frac{d}{dr} + \frac{\kappa_\alpha}{r} - \frac{f_\omega}{2M_N} (\partial_r \omega_0(r)) - \frac{f_\rho}{4M_N} \tau_{0\alpha} (\partial_r R_{0,0}(r)) \right] G_\alpha(r) \\ &\quad + \left[ -M_N + g_\sigma \sigma(r) + g_\omega \omega_0(r) + \frac{1}{2} g_\rho \tau_{0\alpha} R_{0,0}(r) \right. \\ &\quad \left. + \frac{1}{2} e (1 + \tau_{0\alpha}) A_0(r) \right] F_\alpha(r) \end{aligned} \quad (14)$$

and anti-nucleons

$$\begin{aligned} -\bar{E}_\alpha \bar{F}_\alpha(r) &= \left[ \frac{d}{dr} + \frac{\kappa_\alpha}{r} + \frac{f_\omega}{2M_N} (\partial_r \omega_0(r)) + \frac{f_\rho}{4M_N} \bar{\tau}_{0\alpha} (\partial_r R_{0,0}(r)) \right] \bar{G}_\alpha(r) \\ &\quad + \left[ M_N - g_\sigma \sigma(r) + g_\omega \omega_0(r) + \frac{1}{2} g_\rho \bar{\tau}_{0\alpha} R_{0,0}(r) \right. \\ &\quad \left. + \frac{1}{2} e (1 - \bar{\tau}_{0\alpha}) A_0(r) \right] \bar{F}_\alpha(r), \end{aligned} \quad (15)$$

$$\begin{aligned} -\bar{E}_\alpha \bar{G}_\alpha(r) &= \left[ -\frac{d}{dr} + \frac{\kappa_\alpha}{r} + \frac{f_\omega}{2M_N} (\partial_r \omega_0(r)) + \frac{f_\rho}{4M_N} \bar{\tau}_{0\alpha} (\partial_r R_{0,0}(r)) \right] \bar{F}_\alpha(r) \\ &\quad + \left[ -M_N + g_\sigma \sigma(r) + g_\omega \omega_0(r) + \frac{1}{2} g_\rho \bar{\tau}_{0\alpha} R_{0,0}(r) \right. \\ &\quad \left. + \frac{1}{2} e (1 - \bar{\tau}_{0\alpha}) A_0(r) \right] \bar{G}_\alpha(r), \end{aligned} \quad (16)$$

where

$$\kappa_\alpha = \begin{cases} -(l+1) & \text{for } j = l + \frac{1}{2} \\ l & \text{for } j = l - \frac{1}{2} \end{cases} \quad (17)$$

and  $\bar{\tau}_{0\alpha}$  is the isospin factor of anti-nucleons,  $\bar{\tau}_{0\alpha} = -\tau_{0\alpha}$ . In the numerical solution of the relativistic wave equations one eliminates the small components to obtain the Schrödinger-equivalent equations. For the nucleon we eliminate the lower component while for the anti-nucleon the upper component. By defining the Schrödinger-equivalent effective mass and potentials of the nucleon

$$M_{eff} = E_\alpha + M_N - g_\sigma \sigma(r) - g_\omega \omega_0(r) - \frac{1}{2} g_\rho \tau_{0\alpha} R_{0,0}(r) - \frac{1}{2} e (1 + \tau_{0\alpha}) A_0(r), \quad (18)$$

$$U_{eff} = M_N - g_\sigma \sigma(r) + g_\omega \omega_0(r) + \frac{1}{2} g_\rho \tau_{0\alpha} R_{0,0}(r) + \frac{1}{2} e (1 + \tau_{0\alpha}) A_0(r), \quad (19)$$

$$W(r) = \frac{\kappa_\alpha}{r} - \frac{f_\omega}{2M_N} (\partial_r \omega_0(r)) - \frac{f_\rho}{4M_N} \tau_{0\alpha} (\partial_r R_{0,0}(r)) \quad (20)$$

and the anti-nucleon

$$\bar{M}_{eff} = \bar{E}_\alpha + M_N - g_\sigma \sigma(r) + g_\omega \omega_0(r) - \frac{1}{2} g_\rho \tau_{0\alpha} R_{0,0}(r) + \frac{1}{2} e (1 + \tau_{0\alpha}) A_0(r), \quad (21)$$

$$\bar{U}_{eff} = M_N - g_\sigma \sigma(r) - g_\omega \omega_0(r) + \frac{1}{2} g_\rho \tau_{0\alpha} R_{0,0}(r) - \frac{1}{2} e (1 + \tau_{0\alpha}) A_0(r), \quad (22)$$

$$\bar{W}(r) = \frac{\kappa_\alpha}{r} + \frac{f_\omega}{2M_N} (\partial_r \omega_0(r)) - \frac{f_\rho}{4M_N} \tau_{0\alpha} (\partial_r R_{0,0}(r)), \quad (23)$$

we arrive at the Schrödinger-equivalent equations for the upper component of the nucleon's wave function

$$E_\alpha G_\alpha(r) = \left[ -\frac{d}{dr} + W(r) \right] M_{eff}^{-1} \left[ \frac{d}{dr} + W(r) \right] G_\alpha(r) + U_{eff} G_\alpha(r) \quad (24)$$

and the lower component of the anti-nucleon's wave function

$$\bar{E}_\alpha \bar{G}_\alpha(r) = \left[ -\frac{d}{dr} + \bar{W}(r) \right] \bar{M}_{eff}^{-1} \left[ \frac{d}{dr} + \bar{W}(r) \right] \bar{G}_\alpha(r) + \bar{U}_{eff} \bar{G}_\alpha(r). \quad (25)$$

The small components can be obtained through the following relations

$$F_\alpha(r) = M_{eff}^{-1} \left[ \frac{d}{dr} + W(r) \right] G_\alpha(r), \quad (26)$$

$$\bar{F}_\alpha(r) = -\bar{M}_{eff}^{-1} \left[ \frac{d}{dr} + \bar{W}(r) \right] \bar{G}_\alpha(r). \quad (27)$$

In the above we have changed  $\bar{\tau}_{0\alpha} \rightarrow -\tau_{0\alpha}$ , i.e., now the anti-nucleon has the same isospin factor as the corresponding nucleon. From Eqs. (24) and (25) one finds that the Schrödinger equation of the anti-nucleon has the same form as that of the nucleon. The only difference relies on the definition of the effective mass and potentials, that is, the vector fields change their signs. The so-called *G-parity* comes out automatically.

It's now a suitable place to discuss the orthonormalization condition of the wave functions. In Eq. (9) the annihilation and creation operators of nucleons and anti-nucleons satisfy the usual anticommutation relations. From the equal-time anticommutation relation of the Dirac field operator one can derive the matrix equation for the normalization of the wave functions

$$\sum_{\alpha} \left[ \psi_{\alpha}(\mathbf{x}, t) \psi_{\alpha}^{+}(\mathbf{y}, t) + \psi_{\alpha}^a(\mathbf{x}, t) \psi_{\alpha}^{a+}(\mathbf{y}, t) \right] = \delta(\mathbf{x} - \mathbf{y}). \quad (28)$$

In static case one can eliminate the  $t$  index. The following orthogonal conditions can be obtained from the Dirac wave equations [18]

$$\int d^3x \psi_{\alpha}^{+}(\mathbf{x}) \psi_{\beta}(\mathbf{x}) = 0 \quad \text{if } \alpha \neq \beta, \quad (29)$$

$$\int d^3x \psi_{\alpha}^{a+}(\mathbf{x}) \psi_{\beta}^a(\mathbf{x}) = 0 \quad \text{if } \alpha \neq \beta, \quad (30)$$

$$\int d^3x \psi_{\alpha}^{+}(\mathbf{x}) \psi_{\beta}^a(\mathbf{x}) = 0. \quad (31)$$

Multiplying Eq. (28) on the right with  $\psi_{\alpha}(\mathbf{y})$  or  $\psi_{\alpha}^a(\mathbf{y})$ , it can be found that these wave functions must satisfy the normalization conditions

$$\int d^3y \psi_{\beta}^{+}(\mathbf{y}) \psi_{\alpha}(\mathbf{y}) = \int d^3y \psi_{\beta}^{a+}(\mathbf{y}) \psi_{\alpha}^a(\mathbf{y}) = \delta_{\alpha\beta}. \quad (32)$$

This leads to the orthonormalization conditions for the radial wave functions of nucleons and anti-nucleons

$$\int_0^{\infty} dr [G_{\alpha}(r) G_{\beta}(r) + F_{\alpha}(r) F_{\beta}(r)] = \delta_{\alpha\beta}, \quad (33)$$

$$\int_0^{\infty} dr [\bar{G}_{\alpha}(r) \bar{G}_{\beta}(r) + \bar{F}_{\alpha}(r) \bar{F}_{\beta}(r)] = \delta_{\alpha\beta}, \quad (34)$$

respectively. The single-particle energies of the nucleon and the anti-nucleon can be evaluated as

$$E_{\alpha} = \int_0^{\infty} dr \{ G_{\alpha}(r) \left[ -\frac{d}{dr} + W(r) \right] F_{\alpha}(r) + F_{\alpha}(r) \left[ \frac{d}{dr} + W(r) \right] G_{\alpha}(r) \}$$

$$+G_\alpha(r)U_{eff}G_\alpha(r)-F_\alpha(r)[M_{eff}-E_\alpha]F_\alpha(r)\}, \quad (35)$$

$$\begin{aligned} \bar{E}_\alpha &= \int_0^\infty dr \left\{ -\bar{F}_\alpha(r) \left[ \frac{d}{dr} + \bar{W}(r) \right] \bar{G}_\alpha(r) - \bar{G}_\alpha(r) \left[ -\frac{d}{dr} + \bar{W}(r) \right] \bar{F}_\alpha(r) \right. \\ &\quad \left. + \bar{G}_\alpha(r)\bar{U}_{eff}\bar{G}_\alpha(r) - \bar{F}_\alpha(r) \left[ \bar{M}_{eff} - \bar{E}_\alpha \right] \bar{F}_\alpha(r) \right\}, \end{aligned} \quad (36)$$

which are obtained through the iteration procedure.

The main ingredients in Eqs. (18) - (23) are the meson fields, which are determined by the Laplace equations

$$(\nabla^2 - m_\sigma^2) \sigma(r) = -g_\sigma \rho_S(r) + \frac{1}{2} b \sigma^2(r) + \frac{1}{3!} c \sigma^3(r), \quad (37)$$

$$(\nabla^2 - m_\omega^2) \omega_0(r) = -g_\omega \rho_0(r) - \frac{f_\omega}{2M_N} \rho_0^T(r), \quad (38)$$

$$(\nabla^2 - m_\rho^2) R_{0,0}(r) = -\frac{1}{2} g_\rho \rho_{0,0}(r) - \frac{f_\rho}{4M_N} \rho_{0,0}^T(r), \quad (39)$$

$$\nabla^2 A_0(r) = -e \rho_{Pr,0}(r), \quad (40)$$

and

$$\nabla^2 = \frac{d^2}{dr^2} + \frac{2}{r} \frac{d}{dr} \quad (41)$$

in the case of spherical nuclei. The source terms of the meson-field equations are various densities which, in principle, should contain the contributions both from the Fermi sea and the Dirac sea. Under the mean-field approximation, those densities are formally computed as the expectation values of various bilinear products of field operators in the ground state of the many-body system. For example, a direct calculation of the baryon density gives

$$\begin{aligned} \rho_0 &= \langle \psi_0 | \psi^+ \psi | \psi_0 \rangle \\ &= \sum_{\alpha=1}^A \psi_\alpha^+ \psi_\alpha + \sum_{\alpha=vac} \psi_\alpha^{a+} \psi_\alpha^a, \end{aligned} \quad (42)$$

where the sum on the second term of the last equality runs over all anti-nucleon spectra in the vacuum, and therefore causes divergence. A proper regularization scheme is apparently needed in order to render it to a finite value. Unfortunately, at the situation of finite nuclei it is currently untractable. If one simply cuts off it, the integration of the term with respect to the space doesn't vanish. This violates the baryon number conservation. In

an alternative point of view, the mean fields are taken as a starting point for calculating corrections within the framework of Quantum Hadrodynamics [23]. That is, one drops the second term and includes quantum corrections by means of Feynman diagrams and path-integral methods. Within this scheme, the contributions of the valence nucleons to the densities are computed by adding up wave functions while the contributions of the Dirac sea are taken into account in loop expansions. At the one-loop level the effective action of the system can be written as [24]

$$\begin{aligned} \Gamma = & \int d^4x \left( \frac{1}{2} \partial_\mu \sigma \partial^\mu \sigma - U(\sigma) - \frac{1}{4} \omega_{\mu\nu} \omega^{\mu\nu} + \frac{1}{2} m_\omega^2 \omega_\mu \omega^\mu - \frac{1}{4} \mathbf{R}_{\mu\nu} \cdot \mathbf{R}^{\mu\nu} + \frac{1}{2} m_\rho^2 \mathbf{R}_\mu \cdot \mathbf{R}^\mu \right. \\ & \left. - \frac{1}{4} A_{\mu\nu} A^{\mu\nu} + CT \right) + \Gamma_{\text{valence}} + \frac{i}{2} \hbar \text{Tr} \ln(iD^{-1}) - i\hbar \text{Tr} \ln(iG^{-1}). \end{aligned} \quad (43)$$

Here the  $CT$  are the counterterms.  $\Gamma_{\text{valence}}$  is the contribution from the valence nucleons, which for time-independent background fields is just minus the energy of the valence nucleons. The last two terms in Eq. (43) represent the contributions of the Dirac sea stemming from the one-meson loop and one-nucleon loop, respectively. By means of the derivative expansion technique [17] they can be expressed as

$$\begin{aligned} \Gamma^{(1)}(\sigma) = & \frac{i}{2} \hbar \text{Tr} \ln(iD^{-1}) \\ = & \int d^4x \left( -V_B^{(1)}(\sigma) + \frac{1}{2} Z^{(1)}(\sigma) (\partial_\mu \sigma)^2 + \dots \right), \end{aligned} \quad (44)$$

$$\begin{aligned} \Gamma^{(1)}(\psi) = & -i\hbar \text{Tr} \ln(iG^{-1}) \\ = & \int d^4x \left( -V_F^{(1)}(\sigma) + \frac{1}{2} Z_{1\sigma}^{(1)}(\sigma) (\partial_\mu \sigma)^2 + \frac{1}{4} Z_{1\omega}^{(1)}(\sigma) \omega_{\mu\nu} \omega^{\mu\nu} \right. \\ & \left. + \frac{1}{4} Z_{1A}^{(1)}(\sigma) A_{\mu\nu} A^{\mu\nu} + \dots \right). \end{aligned} \quad (45)$$

It can be verified that the tensor-coupling terms contribute to the higher-order terms in the derivative expansion and have therefore been neglected.  $V_B^{(1)}(\sigma)$  and  $V_F^{(1)}(\sigma)$  are the effective potentials from the one-meson loop and one-nucleon loop, in which the field is a constant,  $\sigma(x) = \sigma_0$ , the same situation as in nuclear matter. These two terms contain divergent part and should be regularized. Through adding suitable counterterms,  $V_B^{(1)}(\sigma)$  and  $V_F^{(1)}(\sigma)$  can be calculated in nuclear matter which turn out to be [25, 26, 1]

$$V_B^{(1)}(\sigma) = \frac{m_\sigma^4}{(8\pi)^2} \left[ \left( 1 + \frac{b\sigma}{m_\sigma^2} + \frac{c\sigma^2}{2m_\sigma^2} \right)^2 \ln \left( 1 + \frac{b\sigma}{m_\sigma^2} + \frac{c\sigma^2}{2m_\sigma^2} \right) - \left( \frac{b\sigma}{m_\sigma^2} + \frac{c\sigma^2}{2m_\sigma^2} \right) \right]$$

$$-\frac{3}{2} \left( \frac{b\sigma}{m_\sigma^2} + \frac{c\sigma^2}{2m_\sigma^2} \right)^2 - \frac{1}{3} \left( \frac{b\sigma}{m_\sigma^2} \right)^2 \left( \frac{b\sigma}{m_\sigma^2} + \frac{3c\sigma^2}{2m_\sigma^2} \right) + \frac{1}{12} \left( \frac{b\sigma}{m_\sigma^2} \right)^4 \Bigg], \quad (46)$$

$$\begin{aligned} V_F^{(1)}(\sigma) = & -\frac{1}{4\pi^2} \left[ (M_N - g_\sigma \sigma)^4 \ln \left( 1 - \frac{g_\sigma \sigma}{M_N} \right) + M_N^3 g_\sigma \sigma - \frac{7}{2} M_N^2 g_\sigma^2 \sigma^2 \right. \\ & \left. + \frac{13}{3} M_N g_\sigma^3 \sigma^3 - \frac{25}{12} g_\sigma^4 \sigma^4 \right]. \end{aligned} \quad (47)$$

The functional coefficients before various derivative terms can be determined in the derivative expansion technique and read as [9, 12]

$$Z^{(1)}(\sigma) = \frac{1}{12} \frac{(b + c\sigma)^2}{16\pi^2 (m_\sigma^2 + b\sigma + \frac{1}{2}c\sigma^2)}, \quad (48)$$

$$Z_{1\sigma}^{(1)}(\sigma) = -\frac{g_\sigma^2}{2\pi^2} \ln \left( \frac{m^*}{M_N} \right), \quad (49)$$

$$Z_{1\omega}^{(1)}(\sigma) = \frac{g_\omega^2}{3\pi^2} \ln \left( \frac{m^*}{M_N} \right), \quad (50)$$

$$Z_{1A}^{(1)}(\sigma) = \frac{e^2}{6\pi^2} \ln \left( \frac{m^*}{M_N} \right). \quad (51)$$

Inserting Eqs. (44) - (51) into Eq. (43) and minimizing the effective action with respect to the corresponding fields, one reveals the meson-field equations as given before, in which  $\Gamma_{\text{valence}}$  constitutes the densities originated from the valence nucleons while  $\Gamma^{(1)}(\sigma)$  and  $\Gamma^{(1)}(\psi)$  compose the densities stemming from the Dirac sea. At the end we obtain concrete expressions of various densities contained in Eqs. (37) - (40)

$$\rho_S(r) = \rho_S^{val}(r) + \rho_S^{sea}(r), \quad (52)$$

$$\rho_0(r) = \rho_0^{val}(r) + \rho_0^{sea}(r), \quad (53)$$

$$\rho_0^T(r) = \rho_0^{T,val}(r), \quad (54)$$

$$\rho_{0,0}(r) = \rho_{0,0}^{val}(r), \quad (55)$$

$$\rho_{0,0}^T(r) = \rho_{0,0}^{T,val}(r), \quad (56)$$

$$\rho_{Pr,0}(r) = \rho_{Pr,0}^{val}(r) + \rho_{Pr,0}^{sea}(r), \quad (57)$$

and

$$\rho_S^{val}(r) = \frac{1}{4\pi r^2} \sum_{\alpha=1}^{\Omega} w_\alpha (2j_\alpha + 1) \left[ G_\alpha^2(r) - F_\alpha^2(r) \right], \quad (58)$$

$$\rho_0^{val}(r) = \frac{1}{4\pi r^2} \sum_{\alpha=1}^{\Omega} w_{\alpha} (2j_{\alpha} + 1) \left[ G_{\alpha}^2(r) + F_{\alpha}^2(r) \right], \quad (59)$$

$$\rho_0^{T, val}(r) = \frac{1}{4\pi r^2} \sum_{\alpha=1}^{\Omega} w_{\alpha} (2j_{\alpha} + 1) 2 \left[ \partial_r G_{\alpha}(r) F_{\alpha}(r) \right], \quad (60)$$

$$\rho_{0,0}^{val}(r) = \frac{1}{4\pi r^2} \sum_{\alpha=1}^{\Omega} w_{\alpha} (2j_{\alpha} + 1) \tau_{0\alpha} \left[ G_{\alpha}^2(r) + F_{\alpha}^2(r) \right], \quad (61)$$

$$\rho_{0,0}^{T, val}(r) = \frac{1}{4\pi r^2} \sum_{\alpha=1}^{\Omega} w_{\alpha} (2j_{\alpha} + 1) \tau_{0\alpha} 2 \left[ \partial_r G_{\alpha}(r) F_{\alpha}(r) \right], \quad (62)$$

$$\rho_{Pr,0}^{val}(r) = \frac{1}{2} \left[ \rho_0^{val}(r) + \rho_{0,0}^{val}(r) \right], \quad (63)$$

$$\begin{aligned} \rho_S^{sea}(r) = & -\frac{1}{g_{\sigma}} \frac{\partial}{\partial \sigma} \left[ V_B^{(1)}(\sigma) + V_F^{(1)}(\sigma) \right] + \frac{1}{2g_{\sigma}} \left[ \frac{\partial}{\partial \sigma} Z^{(1)}(\sigma) \right] \left[ \frac{d}{dr} \sigma(r) \right]^2 \\ & + \frac{1}{g_{\sigma}} Z^{(1)}(\sigma) \left( \frac{d^2}{dr^2} + \frac{2}{r} \frac{d}{dr} \right) \sigma(r) + \frac{g_{\sigma}^2}{4\pi^2 m^*} \left[ \frac{d}{dr} \sigma(r) \right]^2 \\ & - \frac{g_{\sigma}}{2\pi^2} \ln \left( \frac{m^*}{M_N} \right) \left( \frac{d^2}{dr^2} + \frac{2}{r} \frac{d}{dr} \right) \sigma(r) + \frac{g_{\omega}^2}{6\pi^2 m^*} \left[ \frac{d}{dr} \omega_0(r) \right]^2 \\ & + \frac{e^2}{12\pi^2 m^*} \left[ \frac{d}{dr} A_0(r) \right]^2, \end{aligned} \quad (64)$$

$$\rho_0^{sea}(r) = -\frac{g_{\omega}}{3\pi^2} \ln \left( \frac{m^*}{M_N} \right) \left( \frac{d^2}{dr^2} + \frac{2}{r} \frac{d}{dr} \right) \omega_0(r) + \frac{g_{\sigma} g_{\omega}}{3\pi^2 m^*} \left[ \frac{d}{dr} \sigma(r) \right] \left[ \frac{d}{dr} \omega_0(r) \right], \quad (65)$$

$$\begin{aligned} \rho_{Pr,0}^{sea}(r) = & -\frac{e}{6\pi^2} \ln \left( \frac{m^*}{M_N} \right) \left( \frac{d^2}{dr^2} + \frac{2}{r} \frac{d}{dr} \right) A_0(r) + \frac{eg_{\sigma}}{6\pi^2 m^*} \left[ \frac{d}{dr} \sigma(r) \right] \left[ \frac{d}{dr} A_0(r) \right], \end{aligned} \quad (66) \quad (67)$$

where

$$\begin{aligned} \frac{\partial V_B^{(1)}(\sigma)}{\partial \sigma} = & \frac{m_{\sigma}^4}{(8\pi)^2} \left[ 2 \left( 1 + \frac{b\sigma}{m_{\sigma}^2} + \frac{c\sigma^2}{2m_{\sigma}^2} \right) \left( \frac{b}{m_{\sigma}^2} + \frac{c\sigma}{m_{\sigma}^2} \right) \ln \left( 1 + \frac{b\sigma}{m_{\sigma}^2} + \frac{c\sigma^2}{2m_{\sigma}^2} \right) \right. \\ & \left. - 2 \left( \frac{b\sigma}{m_{\sigma}^2} + \frac{c\sigma^2}{2m_{\sigma}^2} \right) \left( \frac{b}{m_{\sigma}^2} + \frac{c\sigma}{m_{\sigma}^2} \right) - \frac{b^2}{m_{\sigma}^6} (b\sigma^2 + 2c\sigma^3) + \frac{b^4}{3m_{\sigma}^8} \sigma^3 \right], \end{aligned} \quad (68)$$

$$\begin{aligned} \frac{\partial V_F^{(1)}(\sigma)}{\partial \sigma} = & -\frac{1}{4\pi^2} \left[ -g_{\sigma} (M_N - g_{\sigma} \sigma)^3 \left( 1 + 4 \ln \left( 1 - \frac{g_{\sigma} \sigma}{M_N} \right) \right) + M_N^3 g_{\sigma} - 7M_N^2 g_{\sigma}^2 \sigma \right. \\ & \left. + 13M_N g_{\sigma}^3 \sigma^2 - \frac{25}{3} g_{\sigma}^4 \sigma^3 \right] \end{aligned} \quad (69)$$

and

$$\frac{\partial Z^{(1)}(\sigma)}{\partial \sigma} = \frac{1}{192\pi^2} \left[ \frac{2c(b + c\sigma)}{(m_{\sigma}^2 + b\sigma + \frac{1}{2}c\sigma^2)} - \frac{(b + c\sigma)^3}{(m_{\sigma}^2 + b\sigma + \frac{1}{2}c\sigma^2)^2} \right]. \quad (70)$$

In order to be able to calculate unclosed-shell nuclei, the occupation number  $w_\alpha$  have been explicitly indicated. Note that  $\rho_0^{sea}(r)$  is a total derivative and thus the baryon number is conserved. The total energy of the system can be written as

$$E = E_{\text{MFT}} + \Delta E, \quad (71)$$

where

$$\begin{aligned} E_{\text{MFT}} &= \sum_{\alpha=1}^{\Omega} w_\alpha E_\alpha - \frac{1}{2} \int d^3x \left[ -g_\sigma \sigma \rho_S + \frac{1}{6} b \sigma^3 + \frac{1}{12} c \sigma^4 + g_\omega \omega_0 \rho_0 \right. \\ &\quad \left. + \frac{f_\omega}{2M_N} \omega_0 \rho_0^T + \frac{1}{2} g_\rho R_{0,0} \rho_{0,0} + \frac{f_\rho}{4M_N} R_{0,0} \rho_{0,0}^T + e A_0 \rho_{Pr,0} \right], \end{aligned} \quad (72)$$

$$\begin{aligned} \Delta E &= \int d^3x \left[ V_B^{(1)}(\sigma) + V_F^{(1)}(\sigma) + \frac{1}{2} Z^{(1)}(\sigma) (\nabla \sigma)^2 - \frac{g_\sigma^2}{4\pi^2} \ln \left( \frac{m^*}{M_N} \right) (\nabla \sigma)^2 \right. \\ &\quad \left. + \frac{g_\omega^2}{6\pi^2} \ln \left( \frac{m^*}{M_N} \right) (\nabla \omega_0)^2 + \frac{e^2}{12\pi^2} \ln \left( \frac{m^*}{M_N} \right) (\nabla A_0)^2 \right]. \end{aligned} \quad (73)$$

The pairing energy and the center-of-mass correction to the total energy are taken into account as elucidated in Ref. [3]. The energy density of homogeneous nuclear matter can be obtained through reducing the above formulae. The compressibility at saturation density reads as

$$\begin{aligned} \frac{1}{9} K &= \frac{g_\omega^2}{m_\omega^2} \rho_0 + \frac{k_F^2}{3(k_F^2 + m^{*2})^{1/2}} + \frac{m^{*2} \rho_0}{(k_F^2 + m^{*2})} \\ &\quad \times \left[ -\frac{1}{g_\sigma^2} \frac{\partial^2}{\partial \sigma^2} (U(\sigma) + V_B^{(1)}(\sigma) + V_F^{(1)}(\sigma))_{\sigma=\sigma_0} + \frac{3\rho_0}{(k_F^2 + m^{*2})^{1/2}} - \frac{3\rho_S^{val}}{m^*} \right]^{-1} \end{aligned} \quad (74)$$

where

$$\rho_S^{val} = \frac{4}{(2\pi)^3} \int_0^{k_F} d^3k \frac{m^*}{(\mathbf{k}^2 + m^{*2})^{1/2}}. \quad (75)$$

The double derivatives in the above expression can be easily computed.

### III. NUMERICAL RESULTS AND DISCUSSIONS

Since the densities stemming from the Dirac sea are evaluated within the derivative expansion technique and expressed by means of the mean fields as well as their derivative terms, the wave functions of anti-nucleons are not involved when solving the meson-field

equations. The numerical procedure of the RHA is similar to the one currently used in the RMF [3], except that one more equation for the anti-nucleon is implemented. It goes as follows: in the  $n$ -th iteration step we have arrived at a set of wave functions of nucleons and mean fields. First, we calculate the densities contributed from the valence nucleons by adding up the nucleon wave functions, and the densities originated from the Dirac sea by evaluating the mean fields as well as their derivative terms. Second, we determine the meson fields by solving the Laplace equations of mesons. Third, we use the new meson fields to solve the Schrödinger-equivalent equation of the nucleon. Fourth, we compute the new single-particle energies of nucleons and determine the occupation numbers by adjusting a Fermi surface such that the particle number is conserved. This completes one iteration step. The iteration is continued until the binding energy is stable up to 6 digits. Finally, we apply the known mean fields to solve the Schrödinger-equivalent equation of the anti-nucleon. The equation itself is solved iteratively. The obtained wave functions are used to calculate the single-particle energies of anti-nucleons. The space of anti-nucleons are truncated by the specified principal and angular quantum numbers  $n$  and  $j$  with the guarantee that the calculated single-particle energies of anti-nucleons are converged when the truncated space is extended. We find that the results are insensitive to the exact values of  $n$  and  $j$  provided large enough numbers are given. We have used  $n = 4, j = 9$  for  $^{16}\text{O}$ ;  $n = 5, j = 11$  for  $^{40}\text{Ca}$ ; and  $n = 9, j = 19$  for  $^{208}\text{Pb}$ .

Table I

The parameters of the model are determined in a least-square fit to the properties of spherical nuclei. The experimental values for the observables used in the fit are given in Table I. The second column gives the measured nuclear binding energies while the last two columns reflect the properties of nuclear shape. In model calculations one can extract the diffraction radius and surface thickness through analyzing the nuclear charge form factor, where the intrinsic nucleon form factors are buried in [3]. Here we just want to note that instead of the commonly used Sachs form factors [27] in the current fitting we have applied recent parameterization of nucleon electromagnetic form factors based

on the Gari-Krümpelmann model [28, 29, 30]. Specifically, we have taken the parameter set of GKex(02S) presented in Ref. [30].

In the fitting processes one can simply forget the anti-nucleon part since the vacuum contributions to the densities are calculated by means of the mean fields and their derivative terms. Once the parameters are specified, we get a set of decided mean fields which are then applied to solve the eigenequation of the anti-nucleon. The eigenfunctions (the wave functions) and eigenvalues (the single-particle energies) of anti-nucleons are the final output of the model calculations. We intend, so to say, to predict the bound states of anti-nucleons through adjusting the model parameters to the bulk properties of finite nuclei.

Compared to the previous version of the RHA model now we have two more parameters  $f_\omega$  and  $f_\rho$  for the tensor couplings of vector mesons. The obtained parameters as well as the corresponding saturation properties are presented in Table II and denoted as the RHAT set. For the sake of comparison we give other two sets of parameters: the NL1 set [3] of the RMF model under the no-sea approximation and the RHA1 set [16] where the vacuum contributions have been taken into account but without tensor-coupling terms. One can see that after introducing the tensor couplings a large effective nucleon mass remains in the RHA model. The value of  $m^*/M_N \approx 0.8$  is close to the one appeared in the Skyrme-force parameterizations for nonrelativistic approaches [19]. Although some rearrangements exist, generally speaking, the changes of parameters between the RHAT set and the RHA1 set are not very significant except that the vector coupling strength  $g_\omega$  is enhanced. This causes a somewhat larger compressibility.

Table II

Table III

In Table III the values of  $\chi^2$  are listed for the three cases and the deviations from the binding energy, diffraction radius and surface thickness are detailed. The spin-orbit splitting in  $^{16}\text{O}$  and the shell fluctuation in  $^{208}\text{Pb}$  are provided together with the empirical values. Obviously, the NL1 set performs a very good fit and describes the spin-orbit interaction satisfactorily. After including the vacuum effects the RHA model still reaches

a reasonable well fit to the bulk properties of spherical nuclei. The effect of tensor-coupling terms induces the spin-orbit force in the RHAT model to be one times larger than that in the RHA1 model, and thus improves the total  $\chi^2$  value. In addition, one can observe an interesting redistribution of deviations between the binding energy and surface thickness. In the RHAT set the  $\chi_E^2$  is suppressed substantially. It indicates an improved fit to the nuclear binding energies as clearly exhibited in Table IV. In the mean time, the contributions from the Dirac sea are enhanced evidently.

Table IV

Fig. 1

The shell fluctuation can typically be expressed via the charge density in  $^{208}\text{Pb}$ . It has been known that both the relativistic and nonrelativistic mean-field theory overestimate  $\delta\rho$  by a factor of 3. From Table III one can find that the NL1 set and the RHAT set share the same disease. However, the RHA1 set reproduces the empirical value quite nicely. Further investigation is needed in order to clarify whether it comes out fortuitously. In Fig. 1 we depict the charge densities of three spherical nuclei reckoned with the RHAT set of parameters. The solid lines represent the experimental data. Except for the amplitude of the shell fluctuations the overall results are in agreement with the data.

Fig. 2

Fig. 3

The contributions of the vacuum to the scalar density and baryon density are shown in Fig. 2. The computations are performed with the RHAT set of parameters for  $^{40}\text{Ca}$ . Noticeable influence from the Dirac sea can be found for the scalar density while the effect on the baryon density is negligible. We have solved the technical problem of fluctuations on the  $\rho_S^{sea}$  met in the previous RHA1 model through making spline extrapolation for the first several points of densities originated from the vacuum. Smooth curves for various densities in different nuclei considered in this work have been obtained. Fig. 3 shows the resultant scalar and vector potentials in  $^{16}\text{O}$  for three models. Due to the vacuum effects the potentials calculated with the RHA model are about half of that computed with the RMF model. After introducing the tensor-coupling terms, the RHAT set receives deeper

potentials compared to the RHA1 set, reflecting the effect of parameter rearrangements. The enhancements are around 20 MeV for S and V in the center of the nucleus, which are nonnegligible on the scale of the nucleon central potential. Especially, the enhancements would be summed up for the anti-nucleon potential rather than cancel each other for the nucleon.

Table V

Table VI

Fig. 4

In Table V and Table VI we present the single-particle energies of protons (neutrons) and anti-protons (anti-neutrons) in three spherical nuclei of  $^{16}\text{O}$ ,  $^{40}\text{Ca}$  and  $^{208}\text{Pb}$ . The binding energies per nucleon and the *rms* charge radii are given too. The experimental data are taken from Ref. [31]. Both the relativistic mean-field theory (NL1) under the no-sea approximation and the relativistic Hartree approach (RHA1, RHAT) taking into account the vacuum contributions can reproduce the observed binding energies and *rms* charge radii quite well. With respect to the large error bars in measurements of the  $1s$  proton (neutron) levels, the results of all three sets of parameters coincide with the data. Because of the large effective nucleon mass, the spin-orbit splitting on the  $1p$  levels is rather small in the RHA1 model. The situation has been ameliorated conspicuously in the current RHAT model incorporating the tensor couplings for the  $\omega$ - and  $\rho$ -meson. At the same time, a large  $m^*$  stays unchanged. The experimental data for the anti-proton (anti-neutron) spectra in the vacuum are presently unavailable. The RMF model and the RHA model provide strikingly different predictions with a deviation of a factor of 2, clearly demonstrating the importance of the Dirac sea effects. On the other hand, the anti-particle energies computed with the RHAT set of parameters are 20 – 30 MeV larger than that reckoned with the RHA1 set, as can be anticipated from Fig. 3. The corresponding proton and anti-proton potentials in  $^{208}\text{Pb}$  are displayed in Fig. 4. The same features observed in the energy spectra are revealed once again.

## VI. SUMMARY AND OUTLOOK

We have incorporated tensor couplings for the  $\omega$ - and  $\rho$ -meson in a relativistic Hartree approach for finite nuclei. After refitting the parameters of the effective Lagrangian to the

bulk properties of spherical nuclei, the spin-orbit force has been enlarged by a factor of 2 compared to the previous version of the RHA model without tensor-coupling terms, while a large effective nucleon mass remains. This improves the total  $\chi^2$  value and brings the computed proton (neutron) spectra more closer to the data. The predicted anti-proton (anti-neutron) spectra in the vacuum are deepened about 20 – 30 MeV. One may argue that the vacuum may not be properly treated by the nucleon degrees of freedom, instead, a quark vacuum may be essential. However, if one speaks about *observing* a vacuum, what one actually means is to measure the response of the vacuum to the laboratory probes. In the environment of a finite nucleus, nucleons are well established physical degrees of freedom, which should be the relevant degrees of freedom for describing the corresponding vacuum too. In the case that a QCD environment is involved, quark degrees of freedom may be necessary.

In view that in the vacuum nucleons and anti-nucleons are always in the form of pairs, one of the promising ways to measure the anti-nucleon spectra in the vacuum of a nucleus is to knock out corresponding nucleons from the bound states emerging from the lower continuum. The incident particles can be photons, electrons or protons. The experimental searches for the vacuum structure have been discussed in detail in Refs. [2, 32]. The dynamical processes can be simulated by using the relativistic Boltzmann-Uehling-Uhlenbeck approach [33, 34, 35, 36] which is a microscopic transport model for single-particle distribution functions. Since the nucleons excited from the bound states of the Dirac sea have to overcome deep potentials in order to become real particles, the final particle spectra as well as the angular distributions should be different to that of nucleons originated from the Fermi sea. Exclusive analyses of observables from the hadron-nucleus reactions at the energy range of several GeV/c will exhibit the structure of quantum vacuum. Work on this aspect is in progress. If the energy of the incident particle is further increased, light nuclei could be directly excited from the vacuum when the correlation effect is taken into account. Relativistic quantum molecular dynamics model [37, 38, 39, 40] is a suitable starting point to study the relevant problems.

It is straightforward to extend the present model to include the hyperon degrees of

freedom. Then one can apply it to investigate the properties of hypernuclei with the effects of quantum vacuum taken into account. As a first step we consider the single- $\Lambda$  and double- $\Lambda$  hypernuclei. Through systematically studying the  $\Lambda$  and nucleon spectra in the Fermi sea and the anti- $\Lambda$  and anti-nucleon spectra in the Dirac sea, one can extract important information for the hyperon interaction, which is an active topic of modern nuclear physics [41, 42, 43, 44]. Here the anti- $\Lambda$  spectra in the vacuum act as further constraints to the effective interactions in addition to the usual considered hypernuclei observables. The similar procedure can be performed for the  $\Xi$ - and  $\Sigma$ -hypernuclei. The detailed understanding of the hyperon-hyperon and hyperon-nucleon interactions in dense medium is fundamental for the study of strange particle production and strange particle flow in relativistic heavy-ion collisions [45, 46, 47] as well as the composition and structure of neutron stars in astrophysics [48].

## ACKNOWLEDGMENTS

The author thanks P.-G. Reinhard for stimulating discussions. This work was supported by the National Natural Science Foundation of China under the grant 10275072 and the Research Fund for Returned Overseas Chinese Scholars.

## References

- [1] B. D. Serot and J. D. Walecka, *Adv. Nucl. Phys.* **16**, 1 (1986).
- [2] N. Auerbach, A.S. Goldhaber, M.B. Johnson, L.D. Miller, and A. Picklesimer, *Phys. Lett.* **B182**, 221 (1986).
- [3] P.-G. Reinhard, M. Rufa, J. Maruhn, W. Greiner, J. Friedrich, *Z. Phys.* **A323**, 13 (1986); M. Rufa, P.-G. Reinhard, J.A. Maruhn, W. Greiner, M.R. Strayer, *Phys. Rev.* **C38**, 390 (1988).
- [4] Y.K. Gambhir, P. Ring, and A. Thimet, *Ann. Phys.* **198**, 132 (1990).

- [5] Zhongzhou Ren, Z.Y. Zhu, Y.H. Cai, and Gongou Xu, Phys. Lett. **B380**, 241 (1996).
- [6] Y. Sugahara and H. Toki, Nucl. Phys. **A579**, 557 (1994).
- [7] K. Rutz, M. Bender, T. Buervenich, T. Schilling, P.-G. Reinhard, J.A. Maruhn, W. Greiner, Phys. Rev. **C56**, 238 (1997); M. Bender, K. Rutz, P.-G. Reinhard, J.A. Maruhn, W. Greiner, Phys. Rev. **C58**, 2126 (1998); T. Buervenich, K. Rutz, M. Bender, P.-G. Reinhard, J.A. Maruhn, W. Greiner, Eur. Phys. J. **A3**, 139 (1998).
- [8] C.J. Horowitz and B.D. Serot, Phys. Lett. **B140**, 181 (1984).
- [9] R.J. Perry, Phys. Lett. **B182**, 269 (1986); Nucl. Phys. **A467**, 717 (1987).
- [10] D.A. Wasson, Phys. Lett. **B210**, 41 (1988).
- [11] W.R. Fox, Nucl. Phys. **A495**, 463 (1989).
- [12] R.J. Furnstahl and C.E. Price, Phys. Rev. **C40**, 1398 (1989); Phys. Rev. **C41**, 1792 (1990).
- [13] I.G. Bearden, H. Boggild, J. Boissevain et al., Phys. Rev. Lett. **85**, 2681 (2000).
- [14] T.A. Armstrong and the E864 Collaboration, Phys. Rev. Lett. **85**, 2685 (2000).
- [15] A. Bohr and B.R. Mottelson, *Nuclear Structure* (W.A. Benjamin, New York, 1969).
- [16] G. Mao, H. Stöcker, and W. Greiner, Int. J. Mod. Phys. **E8**, 389 (1999); AIP Conf. Proc. **597**, 112 (2001).
- [17] I.J.R. Aitchison and C.M. Fraser, Phys. Lett. **B146**, 63 (1984); O. Cheyette, Phys. Rev. Lett. **55**, 2394 (1985); C.M. Fraser, Z. Phys. **C28**, 101 (1985); L.H. Chan, Phys. Rev. Lett. **54**, 1222 (1985).
- [18] S. Weinberg, *The Quantum Theory of Fields* (University of Cambridge Press, Cambridge, 1995).
- [19] J. Friedrich and P.-G. Reinhard, Phys. Rev. **C33**, 335 (1986).

- [20] J. Boguta and A.R. Bodmer, Nucl. Phys. **A292**, 413 (1977).
- [21] J.D. Bjorken and S.D. Drell, *Relativistic Quantum Mechanics* (McGraw-Hill, New York, 1964); C. Itzykson and J.-B. Zuber, *Quantum Field Theory* (McGraw-Hill, New York, 1980).
- [22] W. Greiner, *Quantum Mechanics* (Springer, Berlin, 1989); *Relativistic Quantum Mechanics* (Springer, Berlin, 1990).
- [23] B.D. Serot and J.D. Walecka, Int. J. Mod. Phys. **E6**, 515 (1997).
- [24] R. Jackiw, Phys. Rev. **D9**, 1686 (1974).
- [25] T.D. Lee and G.C. Wick, Phys. Rev. **D9**, 2291 (1974).
- [26] S.A. Chin, Ann. Phys. **108**, 301 (1977).
- [27] G.G. Simon, Ch. Schmitt, F. Borkowski, and V.H. Walther, Nucl. Phys. **A333**, 381 (1980).
- [28] M.F. Gari and W. Krümpelmann, Phys. Lett. **B274**, 159 (1992); **282**(E), 483 (1992).
- [29] E.L. Lomon, Phys. Rev. **C64**, 035204 (2001).
- [30] E.L. Lomon, Phys. Rev. **C66**, 045501 (2002).
- [31] J.H.E. Mattauch, W. Thiele, and A.H. Wapstra, Nucl. Phys. **67**, 1 (1965); D. Vautherin and D.M. Brink, Phys. Rev. **C5**, 626 (1972); H. de Vries, C.W. de Jager, and C. de Vries. At. Data Nucl. Data Tables **36**, 495 (1987).
- [32] Y. Jin and D.S. Onley, Phys. Rev. **C38**, 813 (1988).
- [33] S. Teis, W. Cassing, T. Maruyama, and U. Mosel, Phys. Rev. **C50**, 388 (1994).
- [34] Che Ming Ko, Qi Li, and Ren Chuan Wang, Phys. Rev. Lett. **59**, 1084 (1987).

- [35] P. Danielewicz, Ann. Phys. **152**, 239 (1984).
- [36] G. Mao, Z. Li, Y. Zhuo, Y. Han, and Z. Yu, Phys. Rev. **C49**, 3137 (1994); G. Mao, nucl-th/0110076.
- [37] J. Aichelin, Phys. Rep. **202**, 233 (1991).
- [38] A. Ono and H. Horiuchi, Phys. Rev. **C53**, 2341 (1996); 2958 (1996).
- [39] A. Bohnet, N. Ohtsuka, J. Aichelin, R. Linden, and A. Fässler, Nucl. Phys. **A494**, 349 (1989); Z.S. Wang, A. Fässler, C. Fuchs, V.S. Uma Maheswari, and D. Kosov, Phys. Rev. Lett. **79**, 4096 (1997).
- [40] S.A. Bass et al., Prog. Part. Nucl. Phys. **41**, 255 (1998); M. Bleicher et al., J. Phys. **G25**, 1859 (1999).
- [41] J. Schaffner, C.B. Dover, A. Gal, C. Greiner, D.J. Millener, and H. Stöcker, Ann. Phys. **235**, 35 (1994).
- [42] I.N. Filikhin and A. Gal, Phys. Rev. **C65**, 041001 (2002).
- [43] E. Hiyama, M. Kamimura, T. Motoba, T. Yamada, and Y. Yamamoto, Phys. Rev. Lett. **85**, 270 (2000).
- [44] A. Ramos, M.J. Vicente-Vacas, and E. Oset, Phys. Rev. **C55**, 735 (1997).
- [45] C.M. Ko, V. Koch, G. Li, Annu. Rev. Nucl. Part. Sci. **47**, 505 (1997); C.M. Ko, J. Phys. **G27**, 327 (2001).
- [46] S.E. Vance and M. Gyulassy, Phys. Rev. Lett. **83**, 1735 (1999).
- [47] Z.S. Wang, A. Fässler, C. Fuchs, and T. Waindzoch, Nucl. Phys. **A645**, 177 (1999).
- [48] N.K. Glendenning, ApJ **293**, 470 (1985); N.K. Glendenning and S.A. Moszkowski, Phys. Rev. Lett. **67**, 2414 (1991).

Table 1: The experimental values for the observables included in the fit, the binding energy  $E_B$ , diffraction radius  $R$  and surface thickness  $\sigma$ . In the last line we also give the adopted errors  $\Delta O_n$  for the fit.

	$E_B$ (MeV)	$R$ (fm)	$\sigma$ (fm)
$^{16}\text{O}$	-127.6	2.777	0.839
$^{40}\text{Ca}$	-342.1	3.845	0.978
$^{48}\text{Ca}$	-416.0	3.964	0.881
$^{58}\text{Ni}$	-506.5	4.356	0.911
$^{90}\text{Zr}$	-783.9	5.040	0.957
$^{116}\text{Sn}$	-988.7	5.537	0.947
$^{124}\text{Sn}$	-1050.0	5.640	0.908
$^{208}\text{Pb}$	-1636.4	6.806	0.900
$\Delta O_n/O_n$	0.2%	0.5%	1.5%

Table 2: Parameters of the RMF and the RHA models as well as the corresponding saturation properties.  $M_N$  and  $m_\rho$  are fixed during the fit.

	NL1	RHA1	RHAT
$M_N$ (MeV)	938.000	938.000	938.000
$m_\sigma$ (MeV)	492.250	458.000	450.000
$m_\omega$ (MeV)	795.359	816.508	814.592
$m_\rho$ (MeV)	763.000	763.000	763.000
$g_\sigma$	10.1377	7.1031	7.0899
$g_\omega$	13.2846	8.8496	9.2215
$g_\rho$	9.9514	10.2070	11.0023
$b$ (fm $^{-1}$ )	24.3448	24.0870	18.9782
$c$	−217.5876	−15.9936	− 27.6894
$f_\omega/M_N$ (fm)	0.0	0.0	2.0618
$f_\rho/M_N$ (fm)	0.0	0.0	45.3318
$\rho_0$ (fm $^{-3}$ )	0.1518	0.1524	0.1493
$E/A$ (MeV)	−16.43	−16.98	− 16.76
$m^*/M_N$	0.572	0.788	0.779
$K$ (MeV)	212	294	311
$a_4$ (MeV)	43.6	40.4	44.0

Table 3: The standard  $\chi^2$  values of the parameterizations given in Table II. The different sources of deviations from the binding energy, diffraction radius and surface thickness are separated. Other observables like the spin-orbit splitting of the  $1p$  level in  $^{16}\text{O}$  for both protons ( $\delta\epsilon_P$ ) and neutrons ( $\delta\epsilon_N$ ), and the shell fluctuation in  $^{208}\text{Pb}$  ( $\delta\rho$ ) are presented too.

	$\chi_E^2$	$\chi_R^2$	$\chi_\sigma^2$	$\chi_{tot}^2$	$\delta\epsilon_P$ (MeV)	$\delta\epsilon_N$ (MeV)	$\delta\rho$ (fm $^{-3}$ )
NL1	21.96	11.78	32.28	66.02	5.99	6.06	-0.0070
RHA1	516.48	39.14	256.69	812.31	1.99	2.00	-0.0030
RHAT	88.53	24.50	444.86	557.88	3.96	4.43	-0.0067
Exp.					5.98	6.07	-0.0023

Table 4: Experimental and theoretical binding energies per nucleon within the RHA model. The vacuum corrections are indicated explicitly.

	RHA1			RHAT	
	Exp.	Theory	Dirac Sea	Theory	Dirac Sea
$^{16}\text{O}$	-7.98	-8.00	1.37	-7.94	1.68
$^{40}\text{Ca}$	-8.55	-8.73	1.43	-8.62	1.74
$^{48}\text{Ca}$	-8.67	-8.51	1.39	-8.61	1.74
$^{58}\text{Ni}$	-8.73	-8.44	1.44	-8.62	1.85
$^{90}\text{Zr}$	-8.71	-8.74	1.42	-8.78	1.76
$^{116}\text{Sn}$	-8.52	-8.61	1.39	-8.52	1.68
$^{124}\text{Sn}$	-8.47	-8.50	1.34	-8.49	1.68
$^{208}\text{Pb}$	-7.87	-7.93	1.30	-7.88	1.62

Table 5: The single-particle energies of both protons and anti-protons as well as the binding energies per nucleon and the *rms* charge radii in  $^{16}\text{O}$ ,  $^{40}\text{Ca}$  and  $^{208}\text{Pb}$ .

	NL1	RHA1	RHAT	Exp.
$^{16}\text{O}$				
$E/A$ (MeV)	8.00	8.00	7.94	7.98
$r_{ch}$ (fm)	2.73	2.66	2.64	2.74
PROTONS				
$1s_{1/2}$ (MeV)	36.18	30.68	31.63	$40 \pm 8$
$1p_{3/2}$ (MeV)	17.31	15.23	16.18	18.4
$1p_{1/2}$ (MeV)	11.32	13.24	12.22	12.1
ANTI-PRO.				
$1\bar{s}_{1/2}$ (MeV)	674.11	299.42	328.55	
$1\bar{p}_{3/2}$ (MeV)	604.70	258.40	283.44	
$1\bar{p}_{1/2}$ (MeV)	605.77	258.93	285.87	
$^{40}\text{Ca}$				
$E/A$ (MeV)	8.58	8.73	8.62	8.55
$r_{ch}$ (fm)	3.48	3.42	3.41	3.45
PROTONS				
$1s_{1/2}$ (MeV)	46.86	36.58	37.01	$50 \pm 11$
$1p_{3/2}$ (MeV)	30.15	25.32	25.95	
$1p_{1/2}$ (MeV)	25.11	24.03	23.63	$34 \pm 6$
ANTI-PRO.				
$1\bar{s}_{1/2}$ (MeV)	796.09	339.83	367.90	
$1\bar{p}_{3/2}$ (MeV)	706.36	309.24	332.10	
$1\bar{p}_{1/2}$ (MeV)	707.86	309.52	333.37	
$^{208}\text{Pb}$				
$E/A$ (MeV)	7.89	7.93	7.88	7.87
$r_{ch}$ (fm)	5.52	5.49	5.46	5.50
PROTONS				
$1s_{1/2}$ (MeV)	50.41	40.80	41.74	
$1p_{3/2}$ (MeV)	44.45	36.45	37.38	
$1p_{1/2}$ (MeV)	43.75	36.21	37.18	
ANTI-PRO.				
$1\bar{s}_{1/2}$ (MeV)	717.01	354.18	377.37	
$1\bar{p}_{3/2}$ (MeV)	705.20	344.48	366.95	
$1\bar{p}_{1/2}$ (MeV)	705.28	344.52	367.24	

Table 6: The single-particle energies of both neutrons and anti-neutrons.

	NL1	RHA1	RHAT	Exp.
<sup>16</sup> O				
NEUTRONS				
1s <sub>1/2</sub> (MeV)	40.21	34.71	35.78	45.7
1p <sub>3/2</sub> (MeV)	21.07	19.04	20.18	21.8
1p <sub>1/2</sub> (MeV)	15.01	17.05	15.75	15.7
ANTI-NEU.				
1s <sub>1/2</sub> (MeV)	667.93	293.23	322.47	
1p <sub>3/2</sub> (MeV)	598.74	252.48	277.94	
1p <sub>1/2</sub> (MeV)	599.74	252.97	279.22	
<sup>40</sup> Ca				
NEUTRONS				
1s <sub>1/2</sub> (MeV)	54.85	44.48	44.98	
1p <sub>3/2</sub> (MeV)	37.79	32.98	33.83	
1p <sub>1/2</sub> (MeV)	32.73	31.71	30.99	
ANTI-NEU.				
1s <sub>1/2</sub> (MeV)	783.87	327.96	355.70	
1p <sub>3/2</sub> (MeV)	694.80	298.04	321.07	
1p <sub>1/2</sub> (MeV)	696.18	298.26	322.15	
<sup>208</sup> Pb				
NEUTRONS				
1s <sub>1/2</sub> (MeV)	58.97	47.40	46.70	
1p <sub>3/2</sub> (MeV)	52.44	42.66	42.31	
1p <sub>1/2</sub> (MeV)	51.82	42.45	41.64	
ANTI-NEU.				
1s <sub>1/2</sub> (MeV)	678.23	313.18	334.39	
1p <sub>3/2</sub> (MeV)	667.70	304.61	325.41	
1p <sub>1/2</sub> (MeV)	667.73	304.61	325.28	

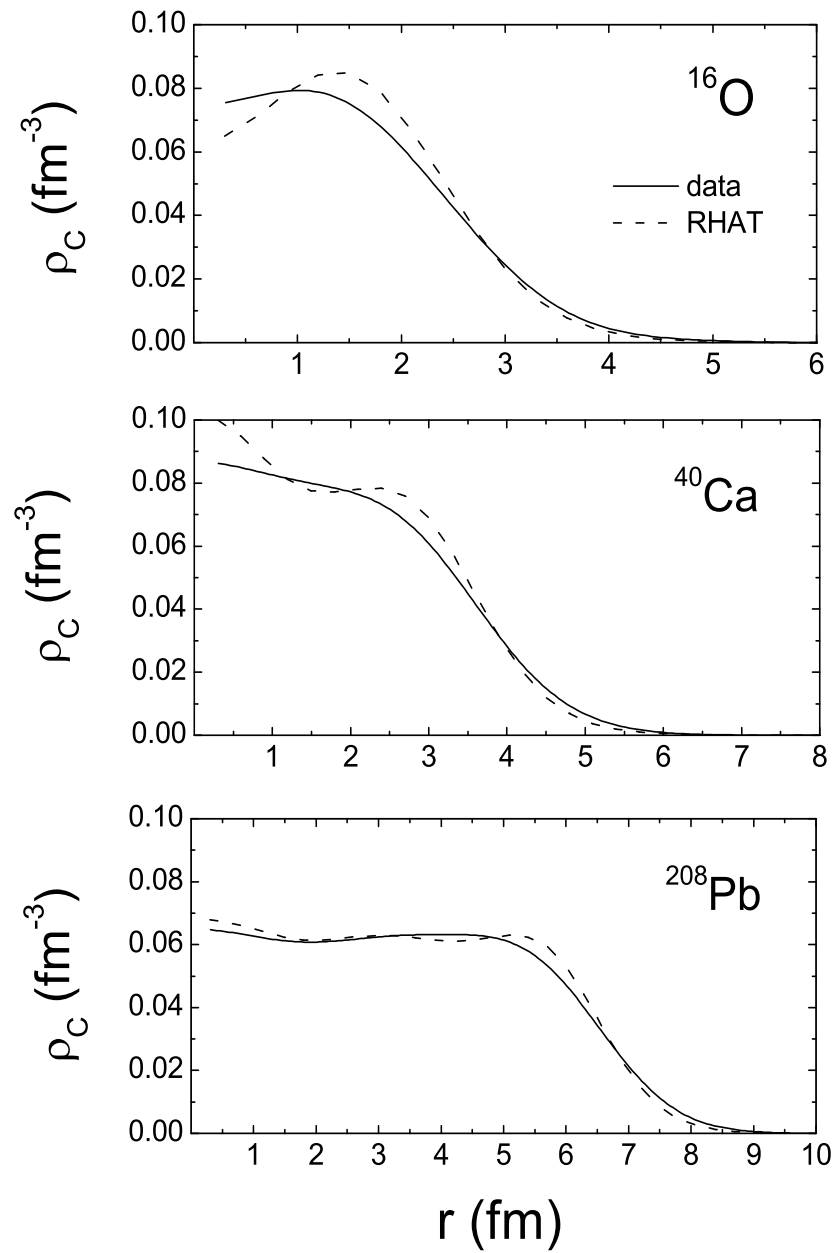


Figure 1: The charge densities in <sup>16</sup>O, <sup>40</sup>Ca and <sup>208</sup>Pb computed with the RHAT set of parameters. The empirical data are depicted as solid lines.

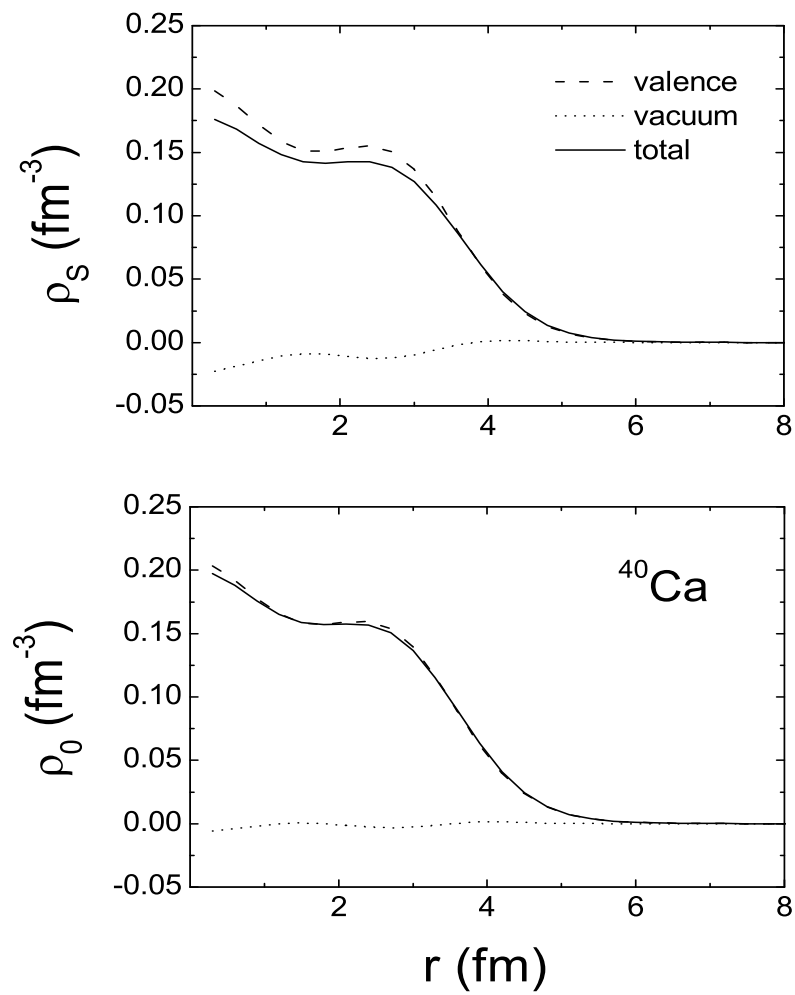


Figure 2: The scalar density and baryon density in  $^{40}\text{Ca}$ . Dashed lines denote the contributions of valence nucleons, dotted lines represent the Dirac-sea effects and solid lines give the total results.

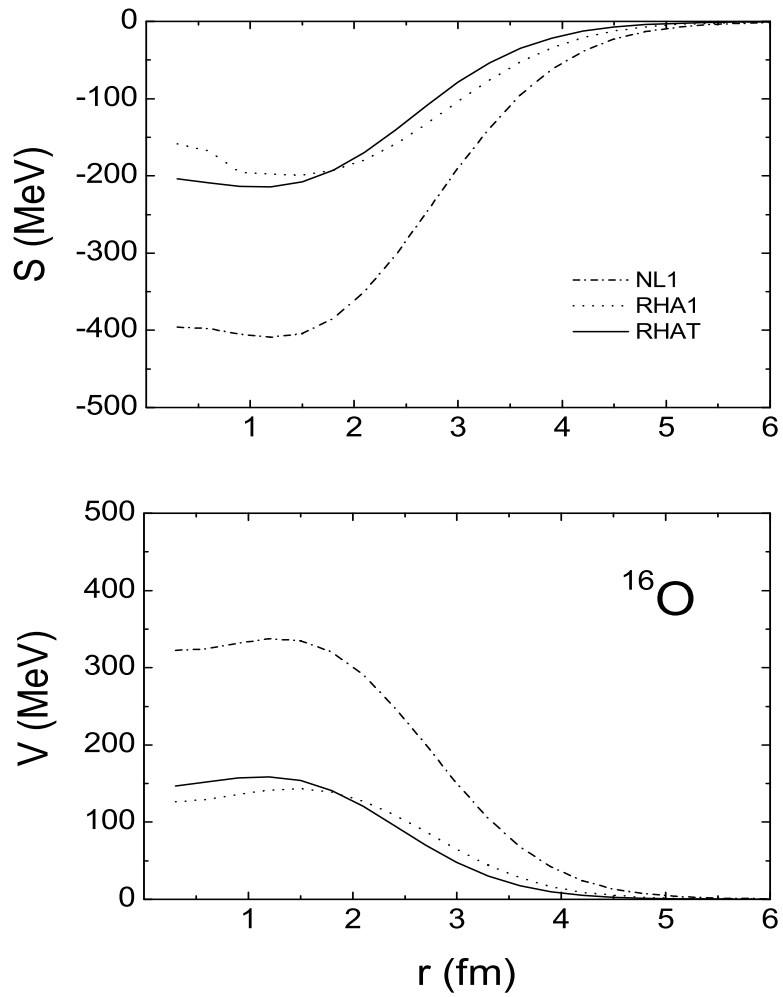


Figure 3: The scalar potential from the  $\sigma$ -meson exchange and the vector potential from the  $\omega$ -meson exchange in  $^{16}\text{O}$ . Different curves are related to different sets of parameters as indicated in the figure.

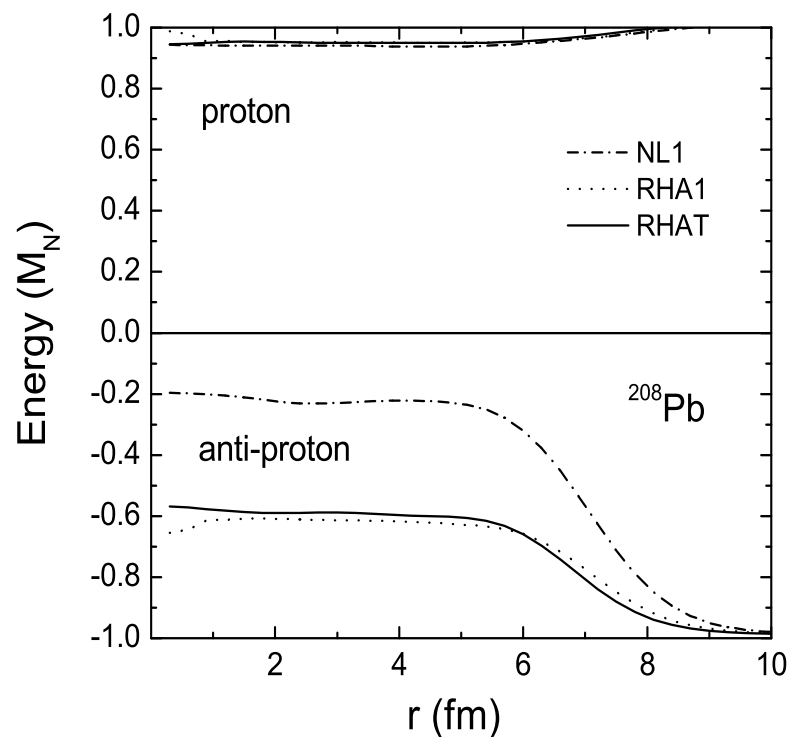


Figure 4: The potentials of the proton and the anti-proton in  $^{208}\text{Pb}$  computed with different sets of parameters as indicated in the figure.